Check for updates

ChemPhysChem

Research Article
doi.org/10.1002/cphc.202300993

Chemistry Europe
European Chemical Societies Publishing

www.chemphyschem.org

# Impact of Vacancy Defects on Electrochemical Nitrogen Reduction Reaction Performance of MXenes

Hardik L. Kagdada*[a] and Ankit Jain[a]

We investigated electrochemical nitrogen reduction reaction (eNRR) on MXenes consisting of the vacancy defects in the functional layer using density functional theory calculations. We considered $Mo_2C$, $W_2C$, $Mo_2N$, and $W_2N$ MXenes with F, N, and O functionalization and investigated distal and alternative associative pathways. We analyzed these MXenes for eNRR based on $N_2$ adsorption energy, $NH_3$ desorption energy, NRR selectivity, and electrochemical limiting potential. While we find that most of the considered MXenes surfaces are more favorable for eNRR compared to hydrogen evolution, these surfaces also have strong $NH_3$ binding ($>-1.0$ eV) and thus will be covered with $NH_3$ during operating conditions. Amongst all considered MXenes, only $W_2NF_2$ is found to have a low $NH_3$ desorption energy along with low eNRR overpotential and selectivity towards eNRR. The obtained eNRR overpotential and $NH_3$ desorption energy on $W_2NF_2$ are superior to those reported for pristine $W_2N_3$ as well as functionalized MXenes.

## Introduction

Ammonia synthesis is an endothermic reaction and is carried out industrially via the Haber-Bosch process on Fe/Ru-based catalysts at high temperatures (300 to 500 °C) and pressures (200 to 300 bar).[1] Due to these harsh operating conditions and the requirement of molecular hydrogen, ammonia production is highly centralized and accounts for around 2% of global energy consumption along with 1.8% of global $CO_2$ emissions.[2–4] It is, therefore, imperative to explore alternatives for the Haber-Bosch process to synthesize $NH_3$ at milder operating conditions. In this regard, the electrochemical nitrogen reduction reaction (eNRR) has gained much attention recently.[5–8] In eNRR, under the application of external potential, the dissolved dinitrogen gas from the electrolyte is first adsorbed on the cathode/catalyst surface and is subsequently protonated to produce ammonia which is then de-adsorbed from the cathode/catalyst surface. The overall reaction efficiency is predominantly governed by the underlying catalyst which ideally should only produce ammonia with no over-potential.

Numerous catalysts such as transition/noble metals[9,10] and their nitrides[11–15]/oxides[11,16,17] have been computationally/experimentally explored for their potential application in eNRR. However, all tested catalysts so far suffer from low faradic efficiency ($<2\%$)[18–20] and low ammonia yield ($<10^{-9}$ mol cm$^{-1}$ s$^{-1}$). The N≡N bond dissociation and the weak adsorption of $N_2$ on the catalyst surface are major bottlenecks for eNRR catalyst performance. The competitive hydrogen evolution reaction (HER) further adds to these challenges under aqueous operating conditions. There is, therefore, a need to identify catalysts that can activate the $N_2$ molecule and facilitate its subsequent protonation while outperforming the competing HER.

MXenes are a class of novel 2D materials that are synthesized by exfoliation of the corresponding bulk MAX phase.[32,33] MXenes are actively tested for their potential applications in various electrochemical processes such as $CO_2$ reduction to hydrocarbon products,[21] HER,[22,23] oxygen reduction/evolution reaction.[24,25] Further, MXenes are also tested for eNRR due to their high electrical conductivity and active sites.[26,27] For instance, Azofra et al. reported that $V_3C_2$ has a promising eNRR performance due to a low limiting kinetic barrier for the transition state between $N_2$ and $N_2H$ on the $V_3C_2$ surface.[28] Shao et al. systematically studied MXenes with $M_2X$ configuration and reported that $Mo_2C$ and $W_2C$ are the most active candidates for the activation of $N_2$ molecules amongst considered MXenes.[29] These computational studies, however, were carried out for bare MXene surfaces while experimentally MXenes are covered with various functional groups (depending on synthesis conditions).[30,31] For functionalized MXenes, Lv et al. proposed a different mechanism for eNRR, where the reaction intermediate captures the hydrogen from the hydroxyl functional surface atoms.[32] The applied negative potential subsequently self-repairs the hydrogen vacancy on the surface.[32] Johnson et al. studied 65 MXenes consisting of bare and functionalized surfaces and filtered out $W_2CH_2$ as an efficient eNRR catalyst based on theoretical overpotential (~0.9 V), stability, and selectivity for eNRR.[11] However, the desorption of $NH_3$ is not considered in this study, which is crucial in determining the poisoning of the catalyst surface during eNRR.[11,33,34] Furthermore, the role of defects in activating the otherwise inactive catalysts was not explored in any of these studies on functionalized MXenes.

For eNRR, the active catalyst sites must have two characteristics: accept a lone pair of electrons and activate the N≡N bond by donating electrons to anti-bonding orbitals.[35–37] From this perspective, the redistribution of electrons via vacancy-defect engineering[36,38] improves the catalyst performance as was

[a] H. L. Kagdada, A. Jain
Mechanical Engineering Department, IIT Bombay,
Mumbai 400076, India
E-mail: hlkagdada@gmail.com
hardik.kagdada@iitb.ac.in



© 2024 Wiley-VCH GmbH

reported for nitrogen vacancies in transition metal nitrides nanosheets.[39,40] Jin et al. reported that nitrogen vacancies in layered 2D MXene $W_2N_3$ create an electron-deficient environment that facilitates nitrogen adsorption along with an accompanying reduction in the electrochemical overpotential. The synthesized catalyst with nitrogen vacancies in $W_2N_3$ resulted in a high Faradic efficiency of ~11% along with yield rates of ~$10^{-11}$ mol cm$^{-1}$ s$^{-1}$ for ammonia production compared to pristine $W_2N_3$ nanosheets,[39] thus suggesting that vacancy defect engineering of MXenes could be a promising strategy for eNRR.

In this work, we explore eNRR on MXenes $Mo_2CT_x$, $W_2CT_x$, $Mo_2NT_x$, and $W_2NT_x$ with vacancy defects in the functional layer ($T_x$). We focus on four basic criteria for eNRR: (i) $N_2$ activation, (ii) limiting potential, (iii) selectivity towards eNRR, and (iv) desorption of $NH_3$ molecules. All criteria are investigated with a combination of DFT and computational hydrogen electrode.[41,42] Based on these basic criteria, we identify $W_2NF_2$ with vacancy defects as a potential efficient catalyst candidate for eNRR.

## Methodology

The density functional theory (DFT) as implemented in the Vienna ab initio simulation package (VASP) is used to obtain the energies for considered MXene surfaces.[43] The projected augmented wave (PAW) method-based pseudopotentials are used with Perdew-Burke-Ernzerhof (PBE) exchange-correlation functional.[44] The plane-wave kinetic energy cutoff is fixed at 550 eV and the Monkhorst-pack electronic wavevector grid of size 14×14×1 is used for the unit cell-based structure relaxation. The total energy and forces are converged to $10^{-6}$ eV and $10^{-4}$ eV/Å, respectively. The adsorption energies of eNRR intermediates are obtained from the basal plane of 3×3×1 supercells. The geometry optimizations of the pristine surface and eNRR reaction intermediates are performed with a 4×4×1 Monkhorst-pack electronic wavevector grid. DFT-D3 van der Waals corrections are used in all calculations[45] along with a vacuum of 15 Å.

The computational hydrogen electrode (CHE) method is used to obtain the electrochemical potential for eNRR on different catalyst surfaces.[46] The free energy change ($\Delta G$) of each reaction step is calculated as:

$$\Delta G = \Delta E + \Delta E_{ZPE} - T\Delta S - neU + 2.302\, k_B T\, pH \quad (1)$$

Here, $\Delta E$, $\Delta E_{ZPE}$ and $T\Delta S$ are differences between the potential energy, zero-point energy (ZPE), and entropy of the reactants and products, respectively, $n$ represents the number of proton-electron pairs in each reaction step, and $U$ is the applied/needed potential. $\Delta E_{ZPE}$-$T\Delta S$ determines the vibrational energy correction to the free energy change and is obtained based on vibrational frequencies of normal modes using the ASE thermochemistry module.[47] For the present work, $pH$ is set to 0 and the applied/needed potential is obtained from the maximum of the free energy difference of the overall reaction, i.e. $U = max(\Delta G)/e$.

## Results and Discussion

The layered structure of MXenes consists of five atomic layers, demonstrated as $T_x$-M-(C or N)-M-$T_x$, as shown in Figure 1(a). We investigated eNRR on $M_2CT_X$ MXenes with M = Mo, W, and $T_x$ = F, N, O, and $M_2NT_X$ MXenes with M = Mo, W and $T_X$ = F, O resulting in a total of 10 configurations. For each configuration, we considered two different functionalization sites: face-centered cubic (fcc) and hexagonal closed pack (hcp). After

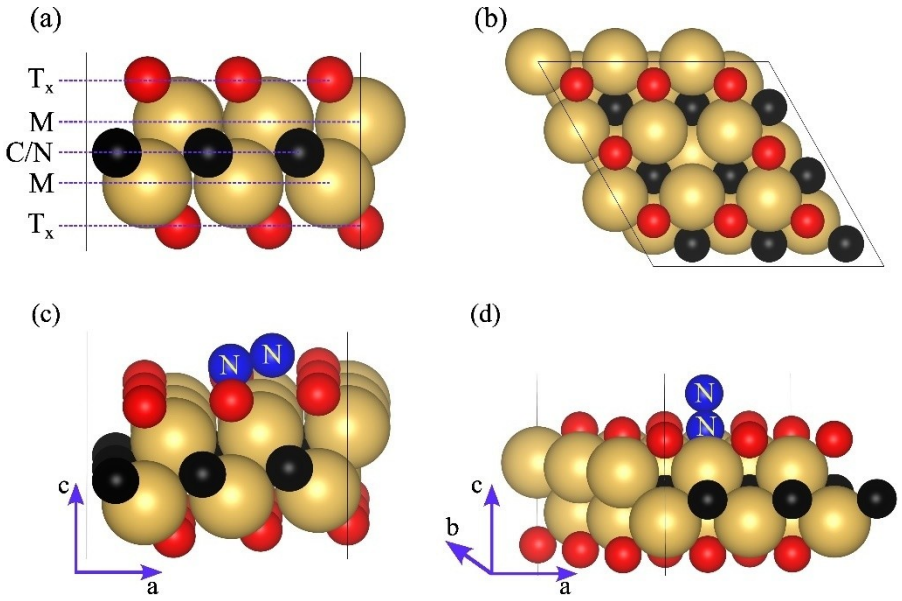


**Figure 1.** (a) The layered structure of MXene consisting of five atomic layers, $T_x$-M–C/N–M-$T_x$, where $T_x$ and M are functional and metal atoms respectively, (b) top view of vacancy defect in functional layer of 3×3 supercell of functional MXene, (c) "side-on", and (d) "end-on" adsorption configuration of $N_2$ over the MXene surface. Missing red atom identifies the the vacancy defect site in the functional layer in (b).


© 2024 Wiley-VCH GmbH

14397641, 0, Downloaded from https://chemistry-europe.onlinelibrary.wiley.com/doi/10.1002/cphc.202300993 by Indian Institute Of Technology, Wiley Online Library on [01/03/2024]. See the Terms and Conditions (https://onlinelibrary.wiley.com/terms-and-conditions) on Wiley Online Library for rules of use; OA articles are governed by the applicable Creative Commons License

structure relaxation, we find that for O functionalization, the fcc site is energetically more stable for all MXenes. For N and F functionalization, other than $W_2CF_2$ for which the fcc site is more stable, the hcp site is energetically more favorable for all MXenes. The vacancy defects are created on the basal plane of these stable configurations by removing one functional atom from the 3×3 supercell as shown in Figure 1(b).

### $N_2$ Activation

For eNRR, $N_2$ adsorption on the defect site of the functional layer is the 1st step in the activation of the N≡N bond. In this regard, we considered two adsorption configurations: "side-on" and "end-on" [Figures 1(c) and 1(d)]. For the side-on configuration, both N atoms from the $N_2$ molecule simultaneously interact with the surface atoms, while for the end-on configuration, one N atom from the $N_2$ molecule interacts with the surface atoms near the defect site. We find that during structure relaxation, the side-on configuration is transitioned into the end-on configuration and, therefore, all adsorption energies are reported for end-on configuration in this work. We find that $N_2$ molecule adsorption energy is negative on all considered defected MXene surfaces, suggesting spontaneous adsorption. The N–N bond length is increased up to 1.163 Å on defected MXenes from 1.113 Å in gas-phase dinitrogen molecules except for $W_2NF_2$, for which the N–N bond length remains unaltered. The negative adsorption energy along with the elongation of the N–N bond length suggests chemo-adsorption of the $N_2$ molecule on defected MXene surfaces.

### eNRR Mechanism

The eNRR can take place through dissociative or associative mechanisms.[48] The first step in the dissociative mechanism is the dissociation of $N_2$, which is followed by the reaction of a proton-electron pair with adsorbed N atoms to produce $2NH_3$ (Figure 2). However, under ambient conditions, electrochemical dissociation of $N_2$ is less favorable owing to the strong energy barrier (~10 eV).[49,50] In the associative mechanism, the $N_2$ molecule is activated first on the catalyst surface and then undergoes subsequent hydrogenation steps. Three possible reaction pathways are possible for associate mechanisms, namely, distal, alternating, and enzymatic pathways (Figure 2). For the associative enzymatic pathway, the $N_2$ should be adsorbed in side-on configuration, while for the alternating and distal pathways, the $N_2$ adsorption should be end-on. As discussed in the previous section, since all considered surfaces exhibit the end-on configuration for $N_2$ adsorption, we have considered only associative distal and alternating mechanisms for eNRR.

For distal and alternating pathways, $*N_2$, *N-NH, $*NH_2$, $NH_3$(g) (* represent the surface), and desorption of $NH_3$ are intermediate reaction steps. For the distal pathway, the farthest N atom from the surface first reacts with proton-electron pairs to produce the $NH_3$ molecule. Subsequently, other N atom passes through the same process to further produce $NH_3$. For the alternative route, both N atoms react alternatively with proton-electron pairs and produce $2NH_3$ in the last two steps of the reaction.

The free energy diagrams for the distal mechanism on considered MXenes are presented in Figure 3 for Mo and W-based MXenes. After $N_2$ activation, the second step is the

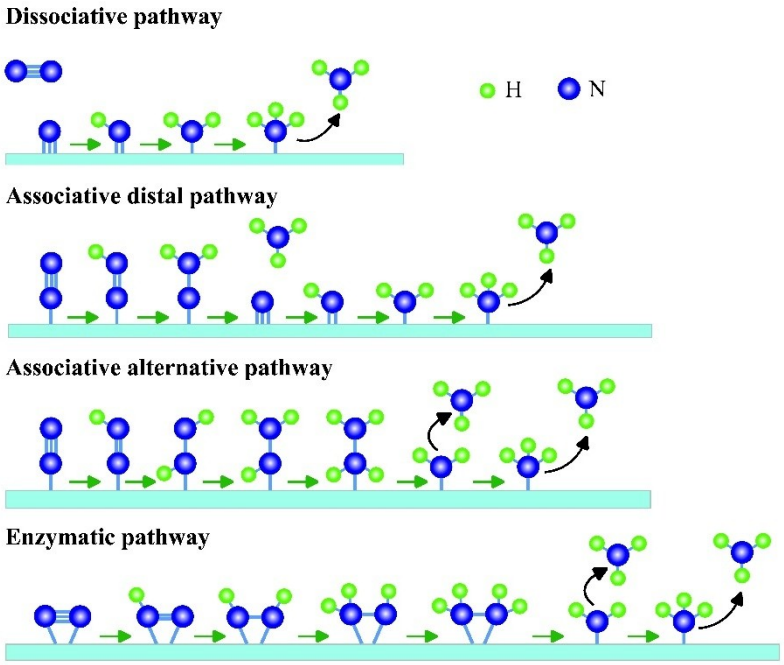


**Figure 2.** Schematic presentation of dissociative and three associative (distal, alternative, and enzymatic) reaction pathways for eNRR.


© 2024 Wiley-VCH GmbH

14397641, 0, Downloaded from https://chemistry-europe.onlinelibrary.wiley.com/doi/10.1002/cphc.202300993 by Indian Institute Of Technology, Wiley Online Library on [01/03/2024]. See the Terms and Conditions (https://onlinelibrary.wiley.com/terms-and-conditions) on Wiley Online Library for rules of use; OA articles are governed by the applicable Creative Commons License

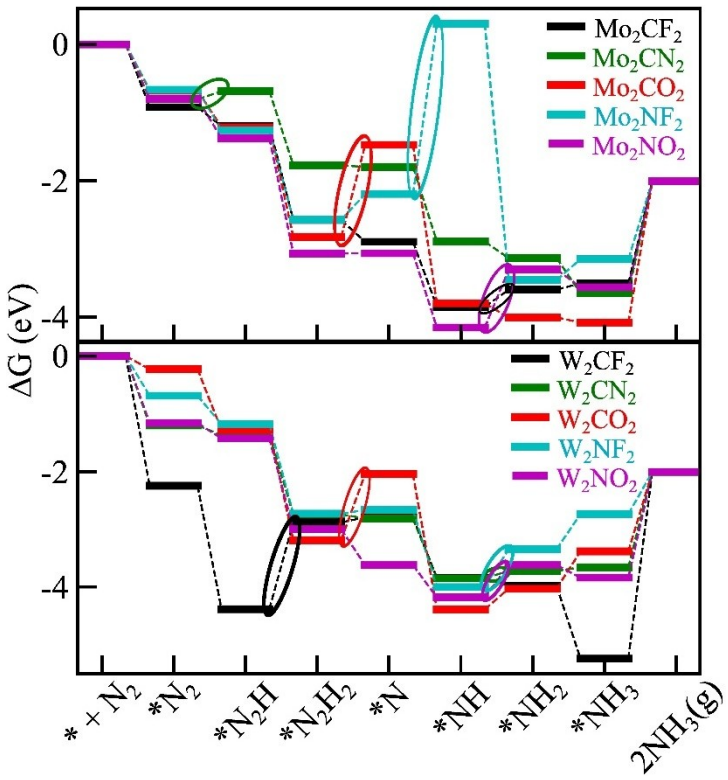


**Figure 3.** Free energy profile of distal eNRR pathways for considered MXenes with no applied potential. Circles between two reaction steps depict the potential determining step.

formation of *N-NH intermediate via the interaction of $*N_2$ with one proton and electron. This elementary step is downhill for all the considered MXenes except for $Mo_2CN_2$. Furthermore, for each hydrogenation step, the bond length between nitrogen atoms gradually increases and such elongation in bond length further helps to release the $NH_3$ molecule and the remaining N atom stays on the surface. For the majority of the considered defected MXenes ($Mo_2CF_2$, $Mo_2NO_2$, $W_2CN_2$ $W_2NF_2$, $W_2NO_2$), the potential limiting step is the formation of $*NH_2$ from *NH, which is the same as that reported for bare $Mo_2C$ and $W_2C$.[11] Amongst remaining MXenes, the formation of *N, *NH, $*N\text{-}NH_2$, and *N intermediates steps are identified as endergonic steps (in $Mo_2CO_2$, $Mo_2NF_2$, $W_2CF_2$, and $W_2CO_2$, respectively).

For the alternating mechanism (Figure 4), the formation of *NHNH from *NNH is the potential determining step for considered MXenes except for $Mo_2CF_2$ and $Mo_2CN_2$. The formation of $*NH_2NH_2$ from $*NHNH_2$ is the potential limiting step for $Mo_2CF_2$. For $Mo_2CN_2$, while the formation of *N-NH and $*NH_2NH_2$ are both uphill in energy, the latter requires more energy.

In the above analysis, we have considered only distal and associative mechanisms, however, in real-time experiments, the reaction could proceed through a more complex pathway involving steps from both distal and alternating mechanisms (referred to as mixed mechanism). We explored mixed pathways for all considered MXenes and report only energetically more favorable (compared to distal/associated pathways) mixed pathways in Figure 5. From the computed energetics, $Mo_2CF_2$,

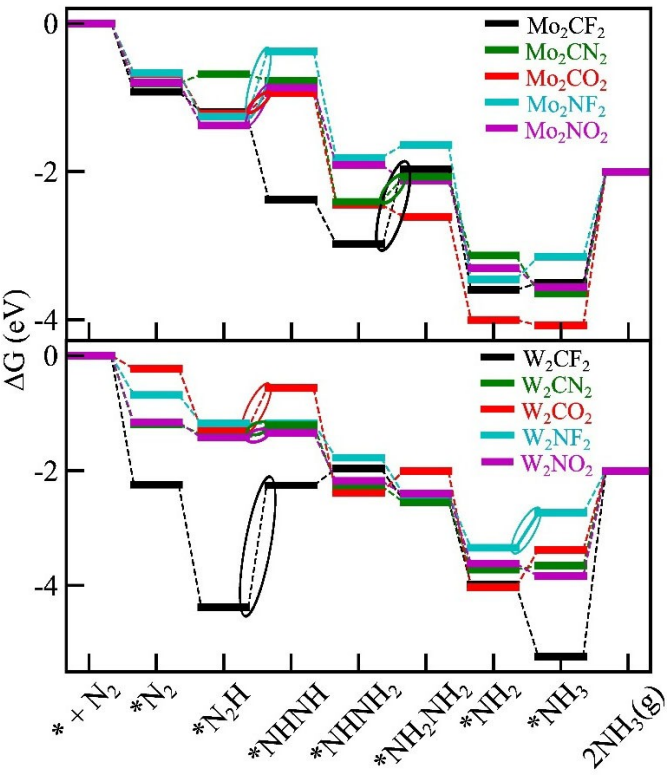


**Figure 4.** Free energy profile of the alternative eNRR pathways for considered MXenes with no potential applied. Circles between consecutive intermediate states depict the potential determining step.


© 2024 Wiley-VCH GmbH

14397641, 0, Downloaded from https://chemistry-europe.onlinelibrary.wiley.com/doi/10.1002/cphc.202300993 by Indian Institute Of Technology, Wiley Online Library on [01/03/2024]. See the Terms and Conditions (https://onlinelibrary.wiley.com/terms-and-conditions) on Wiley Online Library for rules of use; OA articles are governed by the applicable Creative Commons License

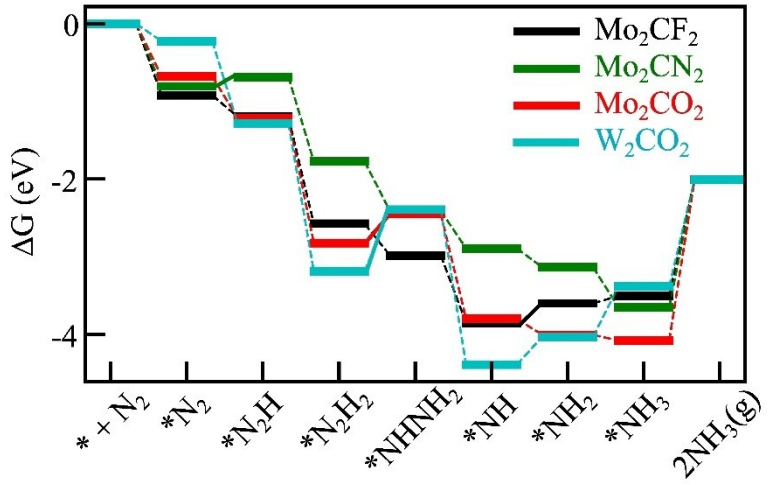


**Figure 5.** Free energy profile of the mixed eNRR pathways for $Mo_2CF_2$, $Mo_2CN_2$, $MO_2CO_2$, and $W_2CO_2$ with no potential applied.

$Mo_2CN_2$, $Mo_2CO_2$, and $W_2CO_2$ favor a mixture of alternative and distal routes. For these systems, the formation of *N-$NH_2$ from *N-NH occurs via the distal mechanism. Subsequently, the alternative mechanism takes over and hydrogen reacts with alternate nitrogen atoms (closest to the surface) to produce intermediate *NH-$NH_2$, and eventually $2NH_3$. For the mixed pathways, however, we find that the computed limiting potentials are similar to that of the alternative mechanism; thus, suggesting that either alternative or mixed pathway could occur for eNRR.

The limiting potentials obtained using distal and alternative paths for considered defected MXenes are summarized in Figure 6. Based on our analysis, we find that eNRR is more likely to proceed through the distal pathway in $Mo_2CF_2$, $Mo_2CN_2$, and $W_2CF_2$. For $W_2CN_2$ and $W_2NF_2$, the obtained limiting potentials are similar for distal and alternative pathways and the reaction could proceed through either pathway. For remaining surfaces, the alternative pathway is more preferred of the two pathways. It is interesting to note that the obtained limiting potentials for all systems are less than −1.0 V via either distal or alternative pathways, except for $W_2CF_2$, thus, suggesting them as potential candidates for eNRR catalyst. Moreover, our obtained limiting potentials for eNRR for these systems are lower than those reported for noble metals[51] and other MXenes.[11,32]

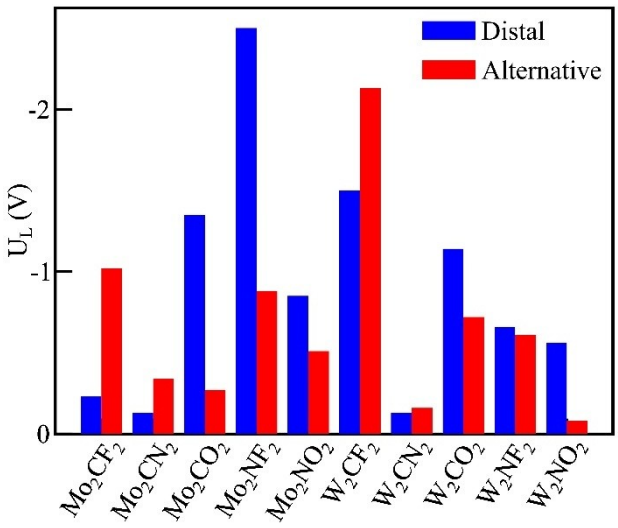


**Figure 6.** Comparison of limiting potential ($U_L$) between distal and alternative pathways.

### Selectivity towards eNRR and HER

HER is a major competing reaction for eNRR and it directly hinders the efficiency of ammonia production in protic solvents. We study the competitive reaction between eNRR and HER by computing the free energy of $N_2$ and H adsorption on considered MXenes surfaces. Our calculations suggest that $Mo_2CN_2$, $Mo_2NO_2$, $W_2CN_2$, and $W_2NO_2$ exhibit lower free energy (more favorable) for *$N_2$ compared to *H. For $Mo_2CF_2$ and $W_2NF_2$, the difference between the free energies of *$N_2$ and *H is less than ~0.2 eV (see Figure 7). Wu et al. reported that electrode potential can influence the charge transfer between Ru from Ru-$N_4$ catalysts and $N_2$.[52] The electron donation from Ru at the reduced potential can promote the activation and adsorption of $N_2$.[52] Therefore, the small adsorption free energy difference between *$N_2$ and *H on $Mo_2CF_2$ and $W_2NF_2$ surfaces can be tuned via applied potential and can result in suppression of HER in a proton limitation environment.

Moreover, the selectivity of eNRR is further determined from the lower limiting potential (i.e. limiting potential close to zero).[32,53] Lv et al. reported that $Mo_2C(OH)_2$ is more favorable for eNRR owing to its lower limiting potential for eNRR than HER, even though OH functionalized MXenes exhibit the "H-poisoning effect".[32] The HER limiting potential has been computed from $\Delta G^*_H/e$, where $\Delta G^*_H$ is the adsorption-free energy of H on the surface. Regardless of the reaction pathways (i.e. considering the low limiting potential pathways), $Mo_2NO_2$ and $W_2CF_2$ are selective for HER owing to their more negative


© 2024 Wiley-VCH GmbH

14397641, 0, Downloaded from https://chemistry-europe.onlinelibrary.wiley.com/doi/10.1002/cphc.202300993 by Indian Institute Of Technology, Wiley Online Library on [01/03/2024]. See the Terms and Conditions (https://onlinelibrary.wiley.com/terms-and-conditions) on Wiley Online Library for rules of use; OA articles are governed by the applicable Creative Commons License

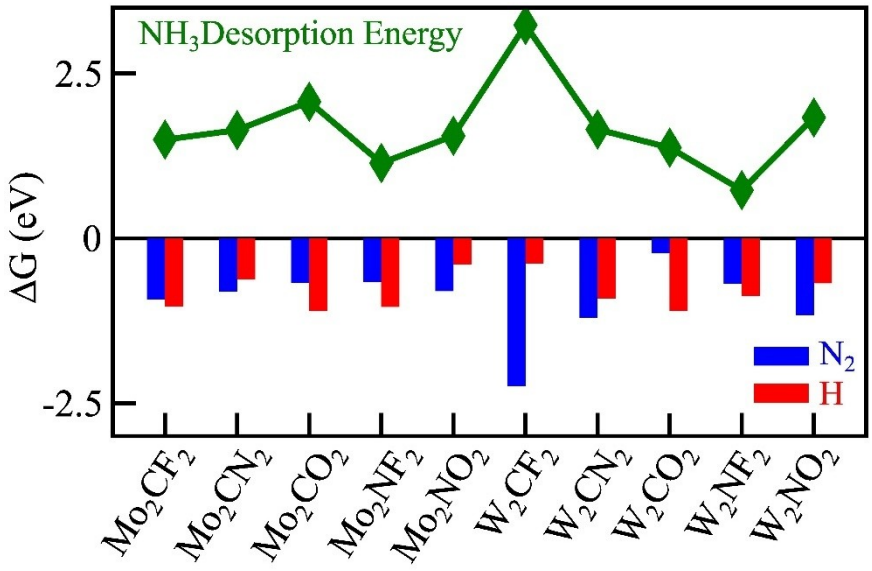


**Figure 7.** The adsorption free energy of $N_2$ and H for eNRR and HER competition on considered MXenes (lower panel) and $NH_3$ desorption energy profile for considered MXenes (upper panel).

limiting potential for HER compared to eNRR potentials, while the rest of the considered MXenes are more favorable for eNRR.

### Desorption of $NH_3$

$NH_3$ desorption is the last step in eNRR and is independent of the reaction pathways. $Mo_2CN_2$, $W_2CN_2$, and $W_2NO_2$ exhibit low values of limiting potential compared to other reported MXenes[11,32] and novel metal surfaces. However, these catalysts exhibit strong poisoning of $NH_3$ owing to the high desorption energy of $NH_3$ (Figure 7). Among considered MXenes, only $W_2NF_2$ has low desorption energy (−0.73 eV) for $NH_3$, along with the low limiting potential and possible selectivity towards the eNRR considering the least negative limiting potential for eNRR.[11,34] Tezak et al established that the desorption energy of $NH_3$ is sensitive to applied bias and decreases with reduced potential while considering the grand canonical density functional theory approach.[54]

The computed desorption energy for $NH_3$ on $W_2NF_2$ is lower than that reported for bare MXenes, while it is slightly higher than OH-functionalized MXenes.[32] Johnson et al[11] suggested that F functionalization improves the eNRR activity compared to O functionalization on MXenes, which is in agreement with our results. Our computed desorption energy and the limiting potential for $W_2NF_2$ are lower than that reported for pristine and nitrogen-vacancy $W_2N_3$ configurations.[39] As such, our computations suggest that $W_2NF_2$ is a better eNRR catalyst than $W_2N_3$ and can result in a superior eNRR performance compared to ~11% FE and −0.97 V overpotential as reported for $W_2N_3$ by Jin et al. [Please cite and ref. [39] here]

## Conclusions

We investigated eNRR on MXenes consisting of vacancy defects in the functional layer by utilizing the density functional theory and computational hydrogen electrode methods. Our study indicates that there is a widespread in the eNRR performance of MXenes with vacancy defects in the functional layer.

The computed limiting potential with single vacancy defects indicates the suitability of considered MXenes for effective eNRR: three considered MXenes ($Mo_2CN_2$, $W_2CN_2$, and $W_2NO_2$) exhibit low limiting potential and high selectivity (compared to HER) towards eNRR, however, the poisoning of $NH_3$ on these MXenes would potentially limit their performance as eNRR electrocatalysts. Considering the balance between selectivity for eNRR, limiting potential, and desorption of $NH_3$, we identified $W_2NF_2$ as the best candidate among the considered defected MXenes [$Mo_2CN_2$, $W_2CN_2$, and $W_2NO_2$]. Moreover, our computations suggest that considered performance parameters are superior for $W_2NF_2$ with F-vacancy defects compared to those reported for $W_2N_3$ with N-vacancy defects. As such, we propose $W_2NF_2$ with F-vacancy defects as a superior eNRR catalyst (compared to all other reported MXene-based catalysts) and urge the experimentalists to further study $W_2NF_2$ for eNRR.

## *Acknowledgements*

The authors acknowledge the funding support from IIT Bombay and Sajjan India Limited, India through Corporate Social Responsibility funding. All calculations were carried out on Space Time-II supercomputing facilities of IIT Bombay.


© 2024 Wiley-VCH GmbH

14397641, 0, Downloaded from https://chemistry-europe.onlinelibrary.wiley.com/doi/10.1002/cphc.202300993 by Indian Institute Of Technology, Wiley Online Library on [01/03/2024]. See the Terms and Conditions (https://onlinelibrary.wiley.com/terms-and-conditions) on Wiley Online Library for rules of use; OA articles are governed by the applicable Creative Commons License

## Conflict of Interests

There are no conflicts of interest to declare

## Data Availability Statement

The data that support the findings of this study are available from the corresponding author upon reasonable request.

**Keywords:** Nitrogen reduction reaction · Mxenes · Functional layer defect · computational hydrogen electrode · catalytic reaction pathways

[1] C. Guo, J. Ran, A. Vasileff, S.-Z. Qiao, *Energy Environ. Sci.* **2018**, *11*, 45–56.
[2] J. Yin, Q. Fan, Y. Li, F. Cheng, P. Zhou, P. Xi, S. Sun, *J. Am. Chem. Soc.* **2016**, *138*, 14546–14549.
[3] M. Kitano, S. Kanbara, Y. Inoue, N. Kuganathan, P. V. Sushko, T. Yokoyama, M. Hara, H. Hosono, *Nat. Commun.* **2015**, *6*, 6731.
[4] B. H. R. Suryanto, K. Matuszek, J. Choi, R. Y. Hodgetts, H.-L. Du, J. M. Bakker, C. S. M. Kang, P. V. Cherepanov, A. N. Simonov, D. R. MacFarlane, *Science (1979)* **2021**, *372*, 1187–1191.
[5] X. Cui, C. Tang, Q. Zhang, *Adv. Energy Mater.* **2018**, *8*, 10.1002/aenm.201800369.
[6] M. A. Shipman, M. D. Symes, *Catal. Today* **2017**, *286*, 57–68.
[7] C. J. M. van der Ham, M. T. M. Koper, D. G. H. Hetterscheid, *Chem. Soc. Rev.* **2014**, *43*, 5183–5191.
[8] V. Kyriakou, I. Garagounis, E. Vasileiou, A. Vourros, M. Stoukides, *Catal. Today* **2017**, *286*, 2–13.
[9] E. Skúlason, T. Bligaard, S. Gudmundsdóttir, F. Studt, J. Rossmeisl, F. Abild-Pedersen, T. Vegge, H. Jónsson, J. K. Nørskov, *Phys. Chem. Chem. Phys.* **2012**, *14*, 1235–1245.
[10] S. Back, Y. Jung, *Phys. Chem. Chem. Phys.* **2016**, *18*, 9161–9166.
[11] L. R. Johnson, S. Sridhar, L. Zhang, K. D. Fredrickson, A. S. Raman, J. Jang, C. Leach, A. Padmanabhan, C. C. Price, N. C. Frey, A. Raizada, V. Rajaraman, S. A. Saiprasad, X. Tang, A. Vojvodic, *ACS Catal.* **2020**, *10*, 253–264.
[12] Q. Li, L. He, C. Sun, X. Zhang, *J. Phys. Chem. C* **2017**, *121*, 27563–27568.
[13] D. G. Sangiovanni, A. B. Mei, L. Hultman, V. Chirita, I. Petrov, J. E. Greene, *J. Phys. Chem. C* **2016**, *120*, 12503–12516.
[14] J. G. Howalt, T. Vegge, *Phys. Chem. Chem. Phys.* **2013**, *15*, 20957.
[15] Y. Abghoui, A. L. Garden, J. G. Howalt, T. Vegge, E. Skúlason, *ACS Catal.* **2016**, *6*, 635–646.
[16] Á. B. Höskuldsson, Y. Abghoui, A. B. Gunnarsdóttir, E. Skúlason, *ACS Sustainable Chem. Eng.* **2017**, *5*, 10327–10333.
[17] K. Niu, L. Chi, J. Rosen, J. Björk, *J. Phys. Chem. Lett.* **2022**, *13*, 2800–2807.
[18] B. H. R. Suryanto, D. Wang, L. M. Azofra, M. Harb, L. Cavallo, R. Jalili, D. R. G. Mitchell, M. Chatti, D. R. MacFarlane, *ACS Energy Lett.* **2019**, *4*, 430–435.
[19] S. Z. Andersen, V. Čolić, S. Yang, J. A. Schwalbe, A. C. Nielander, J. M. McEnaney, K. Enemark-Rasmussen, J. G. Baker, A. R. Singh, B. A. Rohr, M. J. Statt, S. J. Blair, S. Mezzavilla, J. Kibsgaard, P. C. K. Vesborg, M. Cargnello, S. F. Bent, T. F. Jaramillo, I. E. L. Stephens, J. K. Nørskov, I. Chorkendorff, *Nature* **2019**, *570*, 504–508.
[20] B. Izelaar, D. Ripepi, S. Asperti, A. I. Dugulan, R. W. A. Hendrikx, A. J. Böttger, F. M. Mulder, R. Kortlever, *ACS Catal.* **2023**, *13*, 1649–1661.
[21] N. Li, X. Chen, W.-J. Ong, D. R. MacFarlane, X. Zhao, A. K. Cheetham, C. Sun, *ACS Nano* **2017**, *11*, 10825–10833.
[22] Z. W. Seh, K. D. Fredrickson, B. Anasori, J. Kibsgaard, A. L. Strickler, M. R. Lukatskaya, Y. Gogotsi, T. F. Jaramillo, A. Vojvodic, *ACS Energy Lett.* **2016**, *1*, 589–594.
[23] G. Gao, A. P. O'Mullane, A. Du, *ACS Catal.* **2017**, *7*, 494–500.
[24] H. Wang, C. Sun, Y. Cao, J. Zhu, Y. Chen, J. Guo, J. Zhao, Y. Sun, G. Zou, *Carbon N. Y.* **2017**, *114*, 628–634.
[25] T. Y. Ma, J. L. Cao, M. Jaroniec, S. Z. Qiao, *Angew. Chem. Int. Ed.* **2016**, *55*, 1138–1142.
[26] K. R. G. Lim, M. Shekhirev, B. C. Wyatt, B. Anasori, Y. Gogotsi, Z. W. Seh, *Nature Synthesis* **2022**, *1*, 601–614.
[27] M. Naguib, M. Kurtoglu, V. Presser, J. Lu, J. Niu, M. Heon, L. Hultman, Y. Gogotsi, M. W. Barsoum, *Adv. Mater.* **2011**, *23*, 4248–4253.
[28] L. M. Azofra, N. Li, D. R. MacFarlane, C. Sun, *Energy Environ. Sci.* **2016**, *9*, 2545–2549.
[29] M. Shao, Y. Shao, W. Chen, K. L. Ao, R. Tong, Q. Zhu, I. N. Chan, W. F. Ip, X. Shi, H. Pan, *Phys. Chem. Chem. Phys.* **2018**, *20*, 14504–14512.
[30] K. D. Fredrickson, B. Anasori, Z. W. Seh, Y. Gogotsi, A. Vojvodic, *J. Phys. Chem. C* **2016**, *120*, 28432–28440.
[31] M. Naguib, V. N. Mochalin, M. W. Barsoum, Y. Gogotsi, *Adv. Mater.* **2014**, *26*, 992–1005.
[32] X. Lv, L. Kou, T. Frauenheim, *ACS Appl. Mater. Interfaces* **2021**, *13*, 14283–14290.
[33] X. Lv, W. Wei, B. Huang, Y. Dai, T. Frauenheim, *Nano Lett.* **2021**, *21*, 1871–1878.
[34] X. Guo, J. Gu, S. Lin, S. Zhang, Z. Chen, S. Huang, *J. Am. Chem. Soc.* **2020**, *142*, 5709–5721.
[35] H. Tao, C. Choi, L.-X. Ding, Z. Jiang, Z. Han, M. Jia, Q. Fan, Y. Gao, H. Wang, A. W. Robertson, S. Hong, Y. Jung, S. Liu, Z. Sun, *Chem* **2019**, *5*, 204–214.
[36] Y. Fang, Z. Liu, J. Han, Z. Jin, Y. Han, F. Wang, Y. Niu, Y. Wu, Y. Xu, *Adv. Energy Mater.* **2019**, *9*, 10.1002/aenm.201803406.
[37] C. Ling, X. Niu, Q. Li, A. Du, J. Wang, *J. Am. Chem. Soc.* **2018**, *140*, 14161–14168.
[38] Y. Zhang, W. Qiu, Y. Ma, Y. Luo, Z. Tian, G. Cui, F. Xie, L. Chen, T. Li, X. Sun, *ACS Catal.* **2018**, *8*, 8540–8544.
[39] H. Jin, L. Li, X. Liu, C. Tang, W. Xu, S. Chen, L. Song, Y. Zheng, S. Qiao, *Adv. Mater.* **2019**, *31*, 10.1002/adma.201902709.
[40] X. Yang, J. Nash, J. Anibal, M. Dunwell, S. Kattel, E. Stavitski, K. Attenkofer, J. G. Chen, Y. Yan, B. Xu, *J. Am. Chem. Soc.* **2018**, *140*, 13387–13391.
[41] X. Hu, L. Xiong, W.-H. Fang, N. Q. Su, *ACS Appl. Mater. Interfaces* **2022**, *14*, 27861–27872.
[42] S. K. Sahoo, J. Heske, M. Antonietti, Q. Qin, M. Oschatz, T. D. Kühne, *ACS Appl. Energ. Mater.* **2020**, *3*, 10061–10069.
[43] G. Kresse, J. Furthmüller, *Comput. Mater. Sci.* **1996**, *6*, 15–50.
[44] J. P. Perdew, K. Burke, M. Ernzerhof, *Phys. Rev. Lett.* **1996**, *77*, 3865–3868.
[45] S. Grimme, J. Antony, S. Ehrlich, H. Krieg, *J. Chem. Phys.* **2010**, *132*, 10.1063/1.3382344.
[46] J. K. Nørskov, J. Rossmeisl, A. Logadottir, L. Lindqvist, J. R. Kitchin, T. Bligaard, H. Jónsson, *J. Phys. Chem. B* **2004**, *108*, 17886–17892.
[47] A. Hjorth Larsen, J. Jørgen Mortensen, J. Blomqvist, I. E. Castelli, R. Christensen, M. Dułak, J. Friis, M. N. Groves, B. Hammer, C. Hargus, E. D. Hermes, P. C. Jennings, P. Bjerre Jensen, J. Kermode, J. R. Kitchin, E. Leonhard Kolsbjerg, J. Kubal, K. Kaasbjerg, S. Lysgaard, J. Bergmann Maronsson, T. Maxson, T. Olsen, L. Pastewka, A. Peterson, C. Rostgaard, J. Schiøtz, O. Schütt, M. Strange, K. S. Thygesen, T. Vegge, L. Vilhelmsen, M. Walter, Z. Zeng, K. W. Jacobsen, *J. Phys. Condens. Matter* **2017**, *29*, 273002.
[48] S. Liu, Y. Liu, Z. Cheng, Y. Tan, Y. Ren, T. Yuan, Z. Shen, *ACS Appl. Mater. Interfaces* **2021**, *13*, 40590–40601.
[49] A. E. Shilov, *Russ. Chem. Bull.* **2003**, *52*, 2555–2562.
[50] X. Yan, D. Liu, H. Cao, F. Hou, J. Liang, S. X. Dou, *Small Methods* **2019**, *3*, 10.1002/smtd.201800501.
[51] D. Wang, L. M. Azofra, M. Harb, L. Cavallo, X. Zhang, B. H. R. Suryanto, D. R. MacFarlane, *ChemSusChem* **2018**, *11*, 3416–3422.
[52] T. Wu, M. M. Melander, K. Honkala, *ACS Catal.* **2022**, *12*, 2505–2512.
[53] J. H. Montoya, C. Tsai, A. Vojvodic, J. K. Nørskov, *ChemSusChem* **2015**, *8*, 2180–2186.
[54] C. R. Tezak, N. R. Singstock, A. W. Alherz, D. Vigil-Fowler, C. A. Sutton, R. Sundararaman, C. B. Musgrave, *ACS Catal.* **2023**, *13*, 12894–12903.

Manuscript received: December 25, 2023
Revised manuscript received: February 5, 2024
Accepted manuscript online: February 18, 2024
Version of record online: ■■, ■■


© 2024 Wiley-VCH GmbH

14397641, 0, Downloaded from https://chemistry-europe.onlinelibrary.wiley.com/doi/10.1002/cphc.202300993 by Indian Institute Of Technology, Wiley Online Library on [01/03/2024]. See the Terms and Conditions (https://onlinelibrary.wiley.com/terms-and-conditions) on Wiley Online Library for rules of use; OA articles are governed by the applicable Creative Commons License

# RESEARCH ARTICLE

$W_2NF_2$ with F-vacancy defect is a superior electrochemical nitrogen reduction reaction (eNRR) catalyst compared to other MXene-based catalysts, owing to its selectivity towards eNRR, low limiting potential, and low desorption energy for $NH_3$.

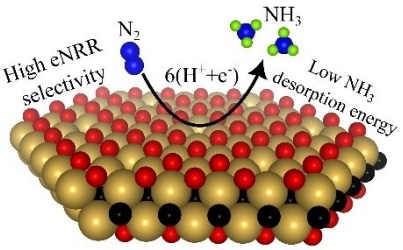


*H. L. Kagdada*, A. Jain*



14397641, 0, Downloaded from https://chemistry-europe.onlinelibrary.wiley.com/doi/10.1002/cptc.202300993 by Indian Institute Of Technology, Wiley Online Library on [01/03/2024]. See the Terms and Conditions (https://onlinelibrary.wiley.com/terms-and-conditions) on Wiley Online Library for rules of use; OA articles are governed by the applicable Creative Commons License